Ab Initio Molecular Dynamics Simulations of the Oxygen Reduction Reaction on a Pt(111) Surface in the Presence of Hydrated Hydronium $(H_3O)^+(H_2O)_2$: Direct or Series Pathway?

Yixuan Wang* and Perla B. Balbuena*

Department of Chemical Engineering, Texas A&M University, 3122 TAMU, College Station, Texas 77843

Received: January 13, 2005; In Final Form: June 11, 2005

Car−Parrinello molecular dynamics simulations have been performed to investigate the oxygen reduction reaction (ORR) on a Pt(111) surface at 350 K. By progressive loading of $(H_3O)^+(H_2O)_{2,3} + e^-$ into a simulation cell containing a Pt slab and O_2 for the first reduction step, and either products or intermediate species for the subsequent reduction steps, the detailed mechanisms of the ORR are well illustrated via monitoring MD trajectories and analyzing Kohn−Sham electronic energies. A proton transfer is found to be involved in the first reduction step; depending on the initial proton−oxygen distance, on the degree of proton hydration, and on the surface charge, such transfer may take place either earlier or later than the O_2 chemisorption, in all cases forming an adsorbed end-on complex H−O−O*. Decomposition of H−O−O* takes place with a rather small barrier, after a short lifetime of approximately 0.15 ps, yielding coadsorbed oxygen and hydroxyl (O* + HO*). Formation of the one-end adsorbed hydrogen peroxide, HOO*H, is observed via the reduction of H−O−O*, which suggests that the ORR may also proceed via HOO*H, i.e., a *series* pathway. However, HOO*H readily dissociates homolytically into two coadsorbed hydroxyls (HO* + HO*) rather than forming a dual adsorbed HOOH. Along the *direct* pathway, the reduction of H−O* + O* yields two possible products, O* + H_2O* and HO* + HO*. Of the three intermediates from the second electron-transfer step, HOO*H from the series pathway has the highest energy, followed by O* + H_2O* and HO* + HO* from the direct pathway. It is therefore theoretically validated that the O_2 reduction on a Pt surface may proceed via a *parallel* pathway, the direct and series occurring simultaneously, with the direct as the dominant step.

1. Introduction

The oxygen reduction reaction (ORR) taking place at the cathode of polymer−electrolyte−membrane fuel cells (PEMFC) has been attracting much attention[1−8] in recent decades because of the desire to elucidate its slow kinetics on electrocatalyst surfaces; this slow kinetics is one of the bottlenecks for achieving improved efficiencies in the fuel cell operation.[9] On the other hand, understanding the ORR mechanisms on a Pt(111) surface, currently known as one of the most active electrocatalysts of PEMFCs, undoubtedly has also significant implications to designing alternative cathode catalysts, aiming to decrease the required amount of the expensive noble metal and to improve the ORR reaction kinetics.

The *overall* ORR on Pt surfaces is a multielectron complex reaction that includes a number of elementary reactions. Yeager proposed two pathways for the overall ORR on Pt(111) in acid medium:[2] (a) a *direct* 4-electron pathway where O_2 is reduced directly to water without involvement of hydrogen peroxide (H_2O_2), $O_2 + 4H^+ + 4e^- \rightarrow 2H_2O$; (b) a *series* 2-electron and 4-electron pathways in which O_2 is reduced to H_2O_2, $O_2 + 2H^+ + 2e^- \rightarrow H_2O_2$, followed by its further reduction, $H_2O_2 + 2H^+ + 2e^- \rightarrow 2H_2O$. It was thereafter suggested that the O_2 reduction on a Pt(111) surface proceeds by a *parallel* pathway, the direct and series mechanisms occurring simultaneously, with the direct as the dominant one.[3] Recent studies from Markovic et al.[10] somewhat favored and suggested that a series pathway via an *adsorbed* H_2O_2 intermediate may apply to Pt- and Pt-based bimetallic catalysts. However, as pointed out by Adzic,[3] if peroxide is not desorbed from the surface before its further reduction, it virtually cannot be detected at ring electrodes, and the direct 4-electron pathway and the series 4-electron pathway are indistinguishable using existing experimental techniques. Not much attempt is made here to review the previous work in detail, but it is necessary to mention that there is still a lack of agreement with respect to the nature of the overall ORR mechanism, which motivates us to perform the present investigation.

Likewise, there are essentially two distinct views regarding the first electron-transfer step. The first view, advocated by Yeager,[11−13] suggested that the most likely mechanism of the direct 4-electron oxygen reduction on Pt(111) surfaces involves dissociative chemisorption of the O_2 molecule on a Pt surface probably accompanied by electron transfer. They also concluded that the dissociative adsorption of O_2 is the rate-determining step (rds) and that the proton transfer follows rather than being involved in the rds.[13] The second view, developed on the basis of the early proposition by Damjanovic et al.,[1,14,15] postulates that proton and charge transfers to the weakly adsorbed O_2 molecule take place simultaneously in the rds: $Pt\cdots O_2 + H_3O^+ + e^- \rightarrow OOH-Pt + H_2O$. This proposal could lead to either a 4-electron direct or series pathway, depending on the fate of the OOH species.

Quantum mechanics provides an alternative way to explore the ORR; theoretical investigations complement state-of-the-art experimental techniques, especially characterizing a variety of intermediates difficult or impossible to be determined by experiments. Taking into account the effect of the electrode potential by matching electron affinity (EA) of the reactants

* Authors to whom correspondence should be addressed. E-mail: yixuan.wang@chemail.tamu.edu (Y.W.); balbuena@tamu.edu (P.B.B.).

10.1021/jp050241z CCC: $30.25
Published on Web 07/15/2005

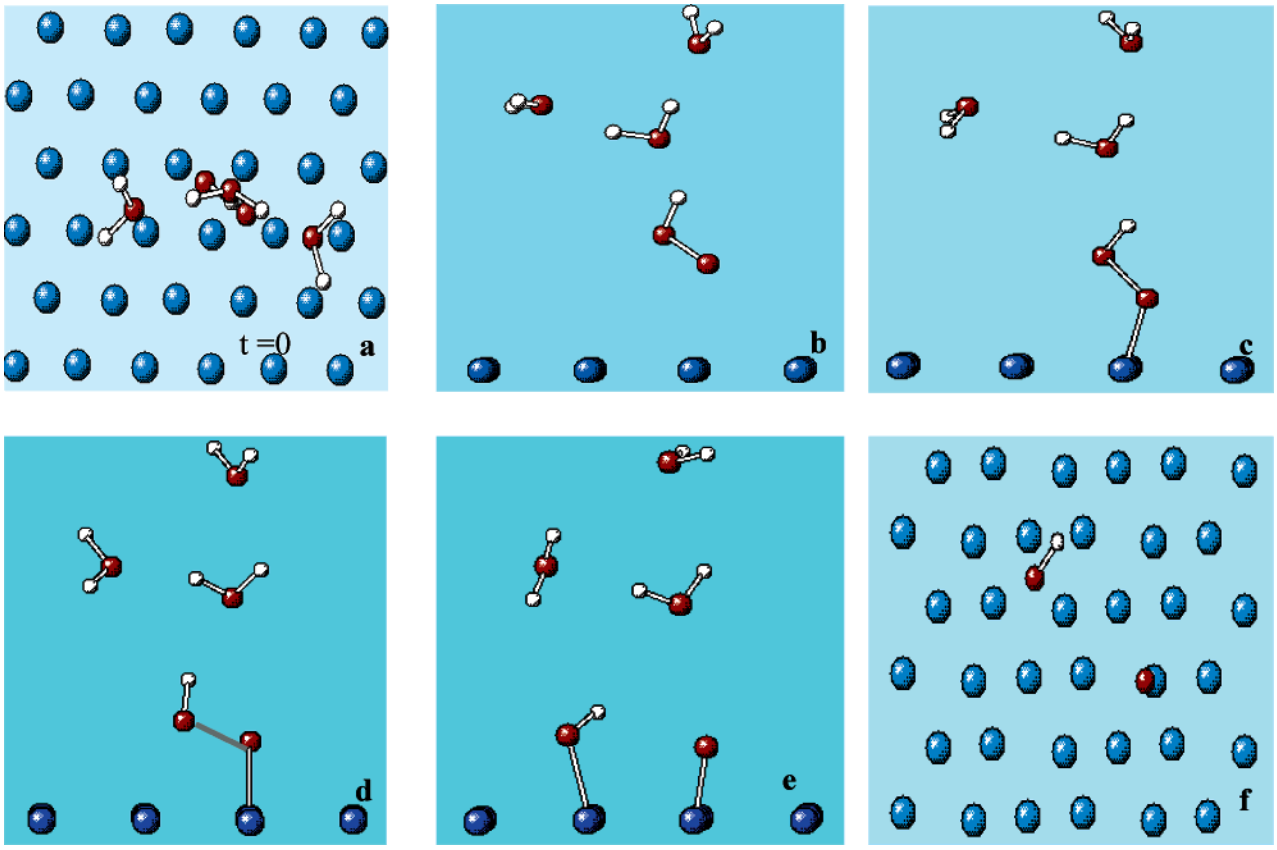

Figure 1. Snapshots from CPMD simulations of (O_2 + H_3O^+ $(H_2O)_2$ + e^-)/Pt(111) at 350 K. For clarity, only the top surface layer is included in (b)−(e). Key: (a) top view of the initial configuration wherein O_2 is located parallel, 3.0 Å above the Pt(111) surface, at a 2-fold bridge site and initial R_{H-O} = 2.2 Å; (b) proton-transfer intermediate at 0.11 ps; (c) end-on chemisorbed species at 0.20 ps, in which the oxygen end is chemisorbed atop while the hydroxyl oxygen is far from the Pt(111) surface, with R_{O-S} = 1.8, R_{HO-S} = 2.6, and R_{O-O} = 1.5 Å and the angle PtOO(H) = 120°; (d) end-on chemisorbed species at 0.36 ps, with R_{O-O} = 1.5 Å and angle PtOO(H) = 110°; (e) atop atomic adsorption at 0.46 ps; (f) oxygen adsorption on top site and hydroxyl adsorption at bridge site at 1.0 ps, with the distances from the hydroxyl oxygen to each of the two Pt atoms being 2.19 and 2.09 Å.

and ionization potential (IP) of the expected product, Anderson et al.[6] used the electron-correlated MP2 method to investigate the O_2 reduction over Pt_2 in the presence of hydrated hydronium representing aqueous acid electrolytes. They found that the proton participates in the first electron-transfer step to form an adsorbed OOH, which basically supports Damjanovic's viewpoint, and that the formation of OOH_{ads} has a considerable energy barrier (0.59 eV at the reversible potential) while the barrier of its dissociation could be negligible (∼0.06 eV). Our previous Car−Parrinello molecular dynamics (CPMD) simulations of the ORR on a Pt(111) surface in the presence of hydrated protons at 350 K basically support their findings.[16] Thus, once it is formed, OOH_{ads} readily decomposes and is unable to yield H_2O_2, which seems to be inconsistent with the experimental findings indicating that certain amount (0−20%, depending on the applied potential) of hydrogen peroxide is formed either as a product or as an intermediate of the ORR on Pt(111) surfaces.[17,18]

By simultaneously solving the Schrödinger equation for the electronic structure in the Kohn−Sham density functional formulation and the nuclei classical equations of motion, ab initio molecular dynamics methods, such as CPMD,[19,20] have the advantage of providing electronic structural information as well as classical molecular dynamics features without the need of an effective force field. In this study, the CPMD method is applied to explore the overall ORR mechanisms. On the basis of CPMD simulations, the sequence of elementary reactions is analyzed in detail, thus allowing the answer to the question if the ORR proceeds in a direct or series pathway. We note that although the reaction mechanism may quantitatively depend on a number of factors, including electrode potential, electrolyte, and adsorbate coverage, the main features of the ORR mechanism may be provided, at least qualitatively, by the present simulations.

2. Computational Details and Model Buildup

All the simulations are performed with the CPMD program, version 3.7.2.[19,20] The code implements density functional theory (DFT) in the Kohn−Sham formulation with a plane-wave basis set and a norm-conserving pseudopotential (PP) for the interactions between the valence electrons and the ionic cores. The DFT method and the PPs used through the present simulation are the BLYP type of generalized-gradient approximation density functional[21,22] and the Troullier and Martins (TM) pseudopotentials,[23] respectively. To accurately treat bond formation and breaking, spin states are polarized. In the TM scheme, Pt has 10 valence electrons ($5d^96s^1$) and O has six ($2s^22p^4$). The wave function is expanded in plane wave basis sets with a kinetic energy cutoff of 70 Ry. Only the Γ-point is used in the Brillouin zone (BZ) sampling generated from the basis vectors of the supercell.

To avoid excessive temperature fluctuations, the Nosé−Hoover thermostat is employed for electrons as well as for ions. The 350 K value is chosen as the target temperature for the ionic system to simulate the PEMFC operational condition. A fictitious electronic mass and a time step are chosen as 600 and 5 au (0.121 fs), respectively. The deuterium mass is used

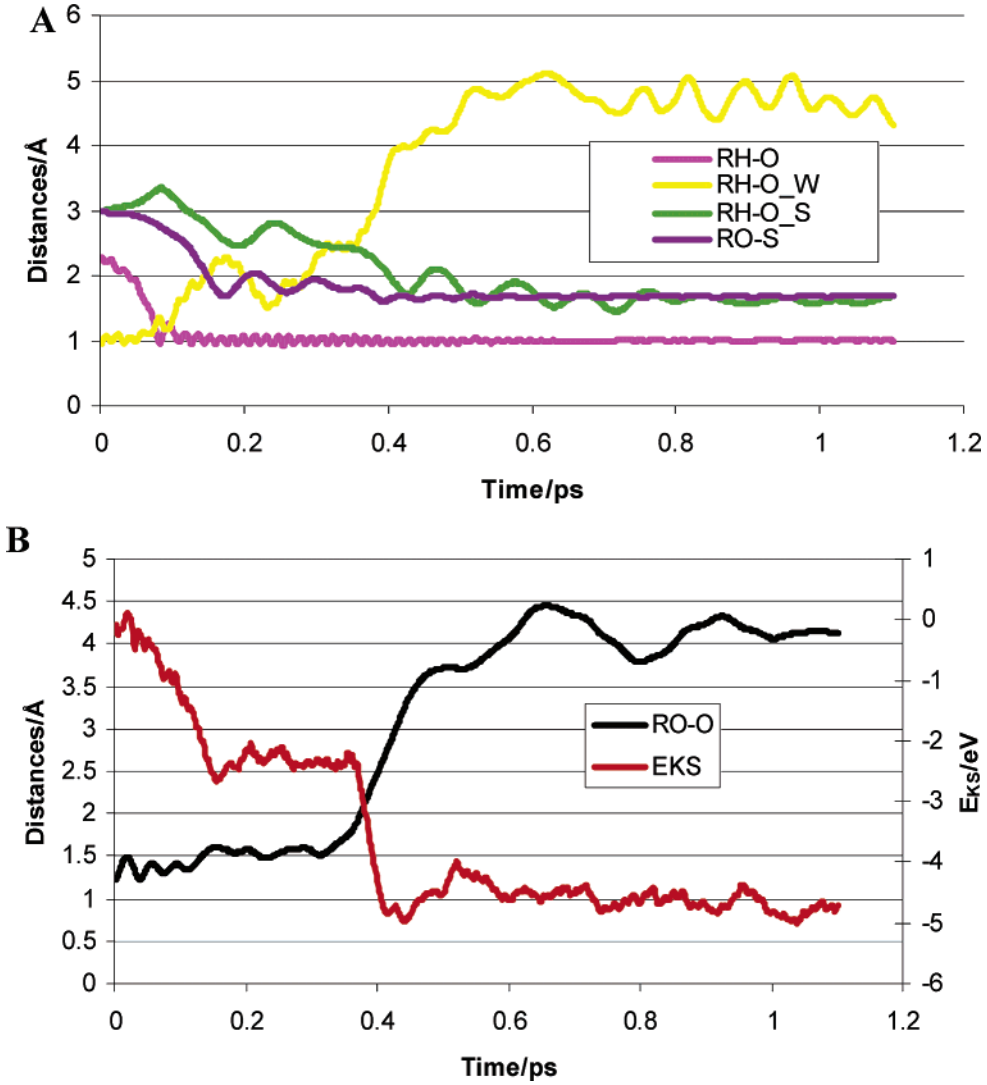

Figure 2. CPMD time evolutions of $(O_2 + H_3O^+(H_2O)_2 + e^-)$/Pt(111) at 350 K with an initial distance from the proton to the closest oxygen atom of O_2 $R_{H-O} = 2.2$ Å: (A) distances from the proton to the closest oxygen atom of O_2 and to the hydronium oxygen (R_{H-O} *and* R_{H-O-W}) and distances from the oxygen and hydroxyl oxygen to the Pt(111) surface (R_{O-S} and R_{HO-S}); (B) Kohn−Sham energy (E_{KS}) and O−O bond length (R_{O-O}).

for the involved hydrogen atoms. The large fictitious electronic mass could help preserve the adiabaticity of the electron dynamics by avoiding a substantial overlap of frequency spectra stemming from the electron and ion dynamics and consequently preventing heating of the electronic systems. To avoid deviations of the potential energy surface from the Born−Oppenheimer (BO) surface, the system is quenched to the BO surface every 1000 steps. In general the system is stable along the BO surface, as evidenced by very small reductions on the order of 0.002 au of the Kohn−Sham energy when the simulations are restarted. Partial atomic charges are estimated by the method of Hirshfeld.[24]

In the CPMD simulations, the system is represented by an orthorhombic supercell with dimensions of 9.58 × 8.30 × 19.22 Å, which contains a three-layer slab of Pt atoms with another seven equivalent layers of vacuum representing the electrolyte region (in the *z*-direction perpendicular to the slab) between any two successive metal slabs. A hydrated hydronium, H_3O^+-$(H_2O)_2$, and O_2 are located in the vacuum space as the initial reactants for the first reduction step, and $H_3O^+(H_2O)_2$ and either the stable products or the intermediates are the species initially present for the subsequent reduction steps. A fully solvated proton, $H^+(H_2O)_4$, is also tested in the first reduction step. Previous calculations have shown that surface relaxation effects are small for extended systems;[25] for this reason the Pt atoms are fixed at their bulk lattice constant (3.912 Å).[26] Each layer of slab contains 12 Pt atoms distributed in a (111) surface. Periodic boundary conditions are employed in all three spatial directions. The electrode potential (U) is equal to the thermodynamic work function ($U/V = \varphi$/eV). The experimental work function of polycrystalline Pt is 5.6 eV;[27] the electrode potential for the current model may correspond to 1.0 V at the standard hydrogen scale.

3. Results and Discussion

3.1. First Electron-Transfer Step: $O_2 + H_3O^+(H_2O)_2 + e^-$ on a Pt(111) Surface. An electrical double layer is believed to exist at the interface between the Pt catalyst and the electrolyte at the electrochemical cell operational conditions. Adsorbates, mainly consisting of oxides and water, lie on the catalyst. It is considered that excess electrons exist on the surface, attracting the H^+ ions from the electrolyte. In an attempt to incorporate such phenomena, the Pt slab is charged by introducing a negative charge to the supercell in all the simulations reported in subsections 3.1.1 and 3.12. Population analysis confirms that

the slab dominantly carries the negative charge in the initial stages of the simulation. In section 3.1.3, we further investigate the effect of the surface charge by removing the excess electron; simulations with a positively charged species are performed with the corresponding negative charge distributed uniformly in the cell.[28]

3.1.1 Effect of the Initial Distance from Proton to O_2. The first electron reduction step is investigated using two typical initial configurations: O_2 is located over a 2-fold bridge (top−bridge−top, Figure 1a) and over a 3-fold fcc hollow (top−hollow−bridge) site, respectively, in a configuration parallel to the slab surface. Each initial configuration is also investigated for different distances from O_2 to the proton of $H_3O^+(H_2O)_2$, (R_{H-O} = 2.2, 2.5, and 3.0 Å in each case), whereas O_2 lies at 3.0 Å from the Pt(111) surface.

Snapshots of a variety of key configurations and Kohn−Sham energies as functions of time are shown for the bridge configuration in Figures 1 and 2, illustrating essential events of the ORR first electron reduction step. Thus, for an initial distance R_{H-O} = 2.2 Å, the hydrated proton gradually migrates toward O_2 and it is still hydrogen bonded by the accompanying water molecule (where the distance between the transferred proton and the water oxygen is $R_{H-O-W} \sim 1.6$ Å) at approximately 0.11 ps (Figure 1b), bringing about a proton-transfer intermediate (H^+-O-O). It is also noted that O_2 rotates from the symmetric bridge site to the remarkably canted top-bridge site and that O_2 is partially polarized due to adsorption (physisorption) to the Pt surface. During the course of this event, the bond length of O_2 (R_{O-O}) elongates to ∼1.40 Å while fluctuating (as shown in Figure 2B) because of the proton effect and the possibly weak interaction between H^+-O-O and the Pt(111) surface. Since the two oxygen atoms are still far from the surface ($R_{HO-S} \sim$ 3.5 Å; $R_{O-S} \sim 2.5$ Å), no clear chemisorption could be expected for $H^+-O-O\cdots$Pt (Figure 1b). With the decrease of R_{HO-S} and R_{O-S} (distances of hydroxyl oxygen and oxygen to the Pt surface), the proton intermediate is then chemisorbed on the Pt(111) surface at 0.18 ps forming an end-on chemisorption species (Figure 1c, H−O−O*, asterisk denoting an adsorption site on the surface thereafter) as postulated by Adzic[29] with the oxygen end having an approximately 1.0 Å shorter distance to the Pt surface than the hydroxyl oxygen (R_{HO-S} = 2.8 Å vs R_{O-S} = 1.8 Å). R_{O-O} increases to around 1.48 Å, and the Kohn−Sham energy (E_{KS}) significantly decreases mainly due to chemisorption of the oxygen end (Figure 2B). Within the following ∼ 0.2 ps, H−O−O* is relaxed on the surface by elongating the R_{O-O} distance and decreasing R_{HO-S}, becoming a decomposition precursor (Figure 1d). The Kohn−Sham energy (Figure 2B) does not change much during this period, indicating that the two opposite contributions to the electronic energy (stretching of the O−O bond and adsorption of HO) balance each other. H−O−O* is most likely to be identified as a top-bridge chemisorption species.

The further reduction of H−O−O* is probably a major channel to generate H_2O_2; the fate of HOO* is therefore of interest to the ORR-related discussion. The lifetime of H−O−O* is approximately 0.2 ps; however, driven by the chemisorption of the hydroxyl, it is noted that the precursor homolytically decomposes into an atop-adsorbed hydroxyl and oxygen via a barrier of approximately 0.2 eV. This approximate barrier is estimated from the E_{KS} evolution shown in Figure 2B, which is accompanied by O−O cleavage of H−O−O*. The Kohn−Sham energy gets an immediate further decrease of ∼2.2 eV as a result of the hydroxyl chemisorption. The chemisorption energy of OH at the bridge and top sites was also estimated to be ∼2.3 eV by periodic DFT calculations.[30] At 0.46 ps, H−O−O* is completely dissociated (R_{O-O} > 2 Å), and both the hydroxyl and oxygen are adsorbed on atop sites. OH thence diffuses to the neighbor bridge site; Figure 2B shows that the diffusion needs to overcome a significant barrier of ∼0.7 eV, whereas the oxygen atom remains at the top site. During the rest of the simulation, OH and O are stable, coadsorbed at the bridge (the distances from the hydroxyl oxygen to the two closest Pt atoms are ∼2.1 Å) and the top sites (the distance of the oxygen to the adsorbing Pt atom ∼ 1.70 Å), respectively. The properties of OH adsorption on Pt(111) may depend on the way the radicals were generated on the surface[31] and also on the degree of coverage.[30] The present result is in line with the previous claim that OH generally binds preferentially at top and bridge sites.[30,32] The charge population analysis indicates that the Pt−O bond is predominantly ionic (e.g., the partial charges of Pt and O are +0.16 and −0.33 e, respectively), which is qualitatively consistent with previous theoretical studies on the basis of either Pt slab or small clusters.[33−36] The net charge of OH is quite small (∼−0.09 e at 0.69 ps), indicating its primary radical characteristics.

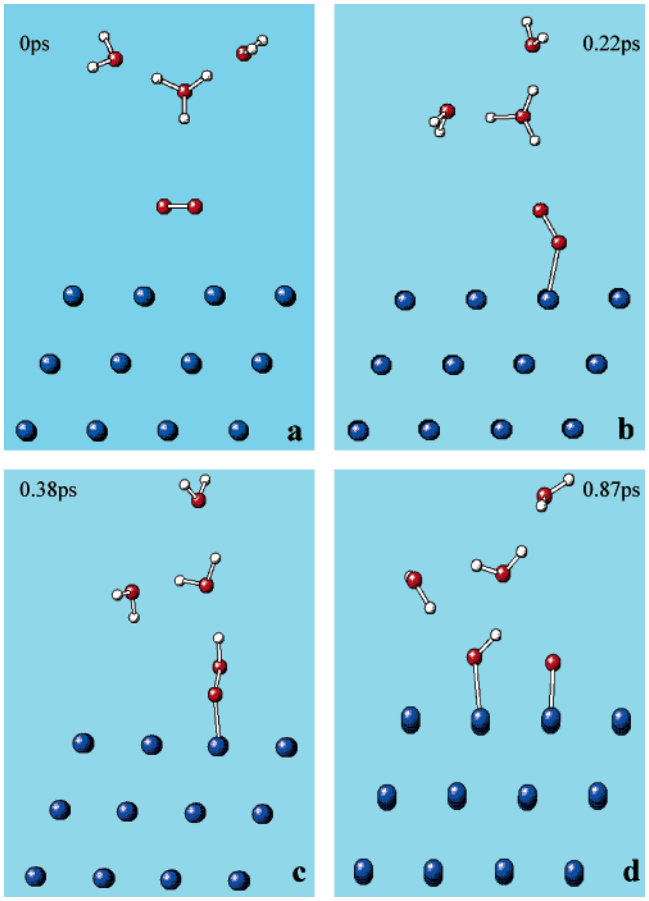

Figure 3. Snapshots from CPMD simulations of (O_2 + $H_3O^+(H_2O)_2$ + e^-)/Pt(111) at 350 K: (a) top view of the initial configuration wherein O_2 is located parallel, 3.0 Å above the Pt(111) surface, at a 2-fold bridge site and initial R_{H-O} = 3.0 Å; (b) chemisorbed O_2 at 0.22 ps; (c) end-on chemisorbed OOH at 0.38 ps; (d) atop atomic adsorption at 0.87 ps.

The essential events for the initial configuration with R_{H-O} = 2.5 Å are very similar to those for the case with R_{H-O} = 2.2 Å. However, when R_{H-O} is further increased to R_{H-O} = 3.0 Å, the *opposite* sequence was found for the chemisorption of O_2 and proton transfer. Figure 3 shows that O_2 gets first chemisorbed until 0.22 ps; this adsorption is accompanied by a drastic decrease of the Kohn−Sham energy and by an approximate 0.15

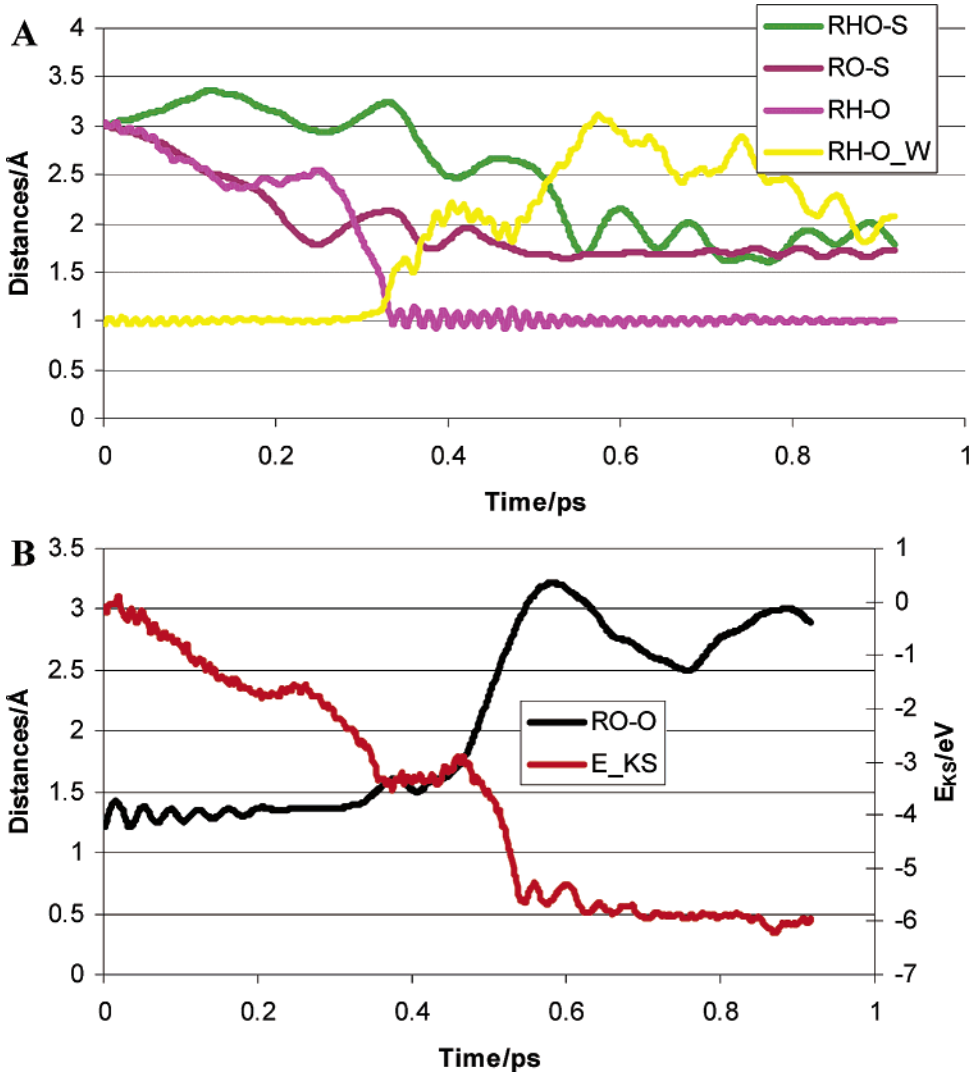

Figure 4. CPMD time evolutions of $(O_2 + H_3O^+(H_2O)_2 + e^-)$/Pt(111) at 350 K with an initial distance from the proton to the closest oxygen atom of O_2 $R_{H-O} = 3.0$ Å: (A) distances from the proton to the closest oxygen atom of O_2 and to the hydronium oxygen (R_{H-O} *and* R_{H-O-W}) and distances from the oxygen and hydroxyl oxygen to the Pt(111) surface (R_{O-S} and R_{HO-S}); (B) Kohn−Sham energy (E_{KS}) and O−O bond length (R_{O-O}).

Å stretching of the O−O distance, as shown by Figure 4B. After chemisorption, O_2 is not found to decompose into adsorbed atoms; instead the hydronium proton transfers to the chemisorbed O_2, forming H−O−O* at 0.377 ps and causing a further decrease of E_{KS} (Figure 4B). This suggests that decomposition of the adsorbed O_2 may have higher activation energy than the formation of O*OH. Although the chemisorption of O_2 and the proton transfer have a sequence different from that in the previous cases where the initial distance R_{H-O} between the proton and the oxygen molecule is shorter, the intermediate H−O−O* is generated in all cases. As in the previous cases, again H−O−O* is a short-lived intermediate and readily decomposes into atop-adsorbed hydroxyl and oxygen species. It was observed again that the adsorbed atomic oxygen remains at the top site instead of diffusing into a 3-fold hollow site, which may be attributed to weak hydrogen bonds formed between the atomic oxygen and hydroxyl as well as with water.

In a comparison of the current results with those of our previous study of the first electron transfer with an initial distance $R_{H-O} = 3.0$ Å but with a smaller kinetic cutoff of 50 au,[18] it can be concluded that a low cutoff overestimates the binding between proton and oxygen, causing the proton-transfer intermediate to take place earlier than the chemisorption of OOH.

Another simulation performed with a top−hollow−bridge initial configuration basically provides essential events similar to those found for the bridge initial configuration with the same initial distance $R_{H-O} = 3.0$ Å. O_2 gets chemisorbed, followed by proton transfer forming H−O−O*. The structure of H−O−O* is similar to a top-bridge chemisorption species (the distances between the hydroxyl oxygen and each of the three neighbor Pt atoms are 3.167, 3.700, and 3.974 Å). Once again, it is found that H−O−O* decomposes into atop oxygen and hydroxyl adsorbed species after relaxing for approximately 0.15 ps on the surface.

3.1.2. Solvent Effect on the First Electron-Transfer Step. A fully hydrated hydronium, $H^+(H_2O)_4$, is also used to investigate the solvent effect in the first electron-transfer step. The snapshots in Figure 5 reflect the essential events. In the initial configuration (Figure 5a), the distance between O_2 and the closest proton is around 2.5 Å. In contrast to the case of $H^+(H_2O)_3$ with initial $R_{H-O} = 2.5$ Å, the stronger hydration prevents the proton from approaching to the partially polarized O_2 to form a proton-

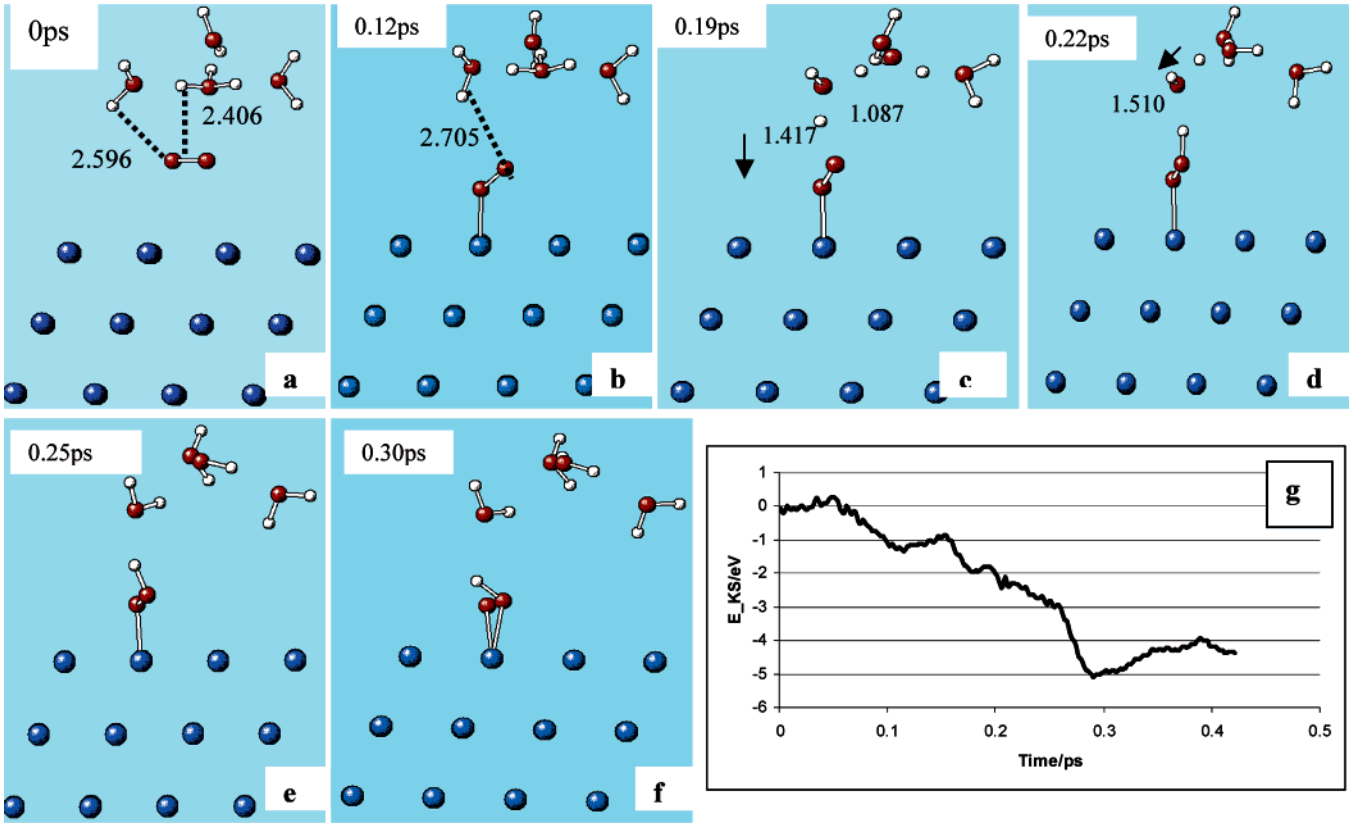

Figure 5. Snapshots and Kohn−Sham energy variation from CPMD simulations of (O_2 + H_3O^+ $(H_2O)_3$ + e^-)/Pt(111) at 350 K: (a) side view of the initial configuration wherein O_2 is located parallel, 3.0 Å above the Pt(111) surface, at a 2-fold bridge site; (b) chemisorbed O_2 at 0.12 ps; (c) proton being transferred from the closest water to the chemisorbed O_2; (d) proton being transferred from hydronium to the water at 0.22 ps; (e) chemisorbed OOH at 0.25 ps; (f) decomposition of the chemisorbed OOH at 0.30 ps; (g) time evolution of the Kohn−Sham energy.

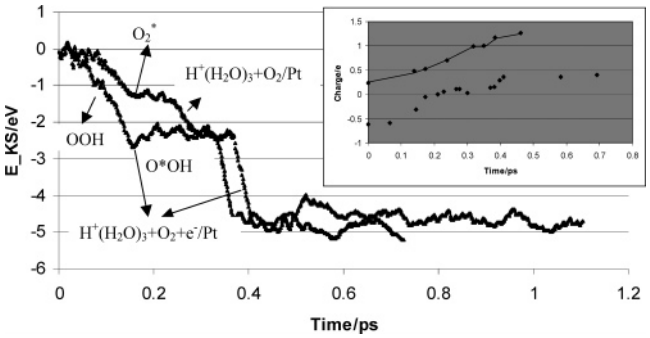

Figure 6. Time evolutions of Kohn−Sham energy from CPMD simulations of (O_2 + H_3O^+ $(H_2O)_3$ + e^-)/Pt(111) and (O_2 + H_3O^+-$(H_2O)_3$)/Pt(111) at 350 K and initial R_{H-O} = 2.5 Å. The inset displays net charges carried by the Pt slab (top line for the cell without added electron; bottom symbols for the cell with electron).

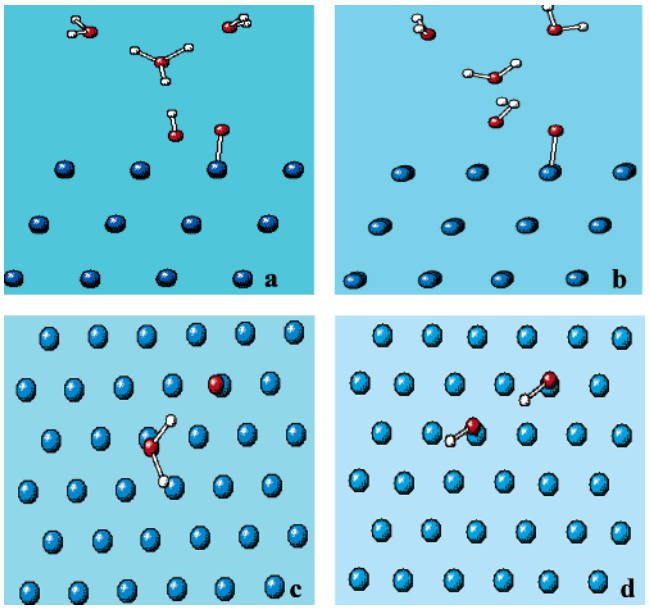

Figure 7. CPMD snapshots of (OH_{ads} + O_{ads} + $H_3O^+(H_2O)_2$ + e^-)/Pt(111) at 350 K: (a) side view of the initial configuration where the hydronium proton is equally separated from the adsorbed oxygen and the hydroxyl oxygen by 2.8 Å; (b) side view of the configuration at 0.065 ps; (c) water dipole nearly parallel to the Pt(111) surface at 0.362 ps; (d) two atop-adsorbed hydroxyls, wherein a hydrogen bond exists at 0.78 ps.

transfer intermediate; instead O_2 gets chemisorbed at 0.12 ps (Figure 5b). Similar to the case of $H^+(H_2O)_3$ with the same initial distance R_{H-O} = 2.5 Å, the chemisorbed O_2 does not dissociate at this stage. It is interesting to note a proton-transfer hopping channel, the proton of water to the chemisorbed O_2 and hydronium proton migrating to water via hydrogen bonds (Figure 5c,d), which yields the end-on adsorbed O*OH at 0.25 ps. According to Figure 5g, the formation of O*OH or the proton transfer need to overcome a barrier of ∼0.4 eV at 0.15 ps. As in all of the previous simulations, O*OH decomposes into adsorbed oxygen and hydroxyl. Here a solvent effect does delay the proton transfer, which clearly occurs after O_2 chemisorption.

3.1.3. Effect of Surface Charge. To address the effect of changes in the electrode potential on the first electron-transfer step, another set of simulations were carried out without the added electron in the simulation cell. To preserve electroneutrality, the positive charge of the proton is counterbalanced by

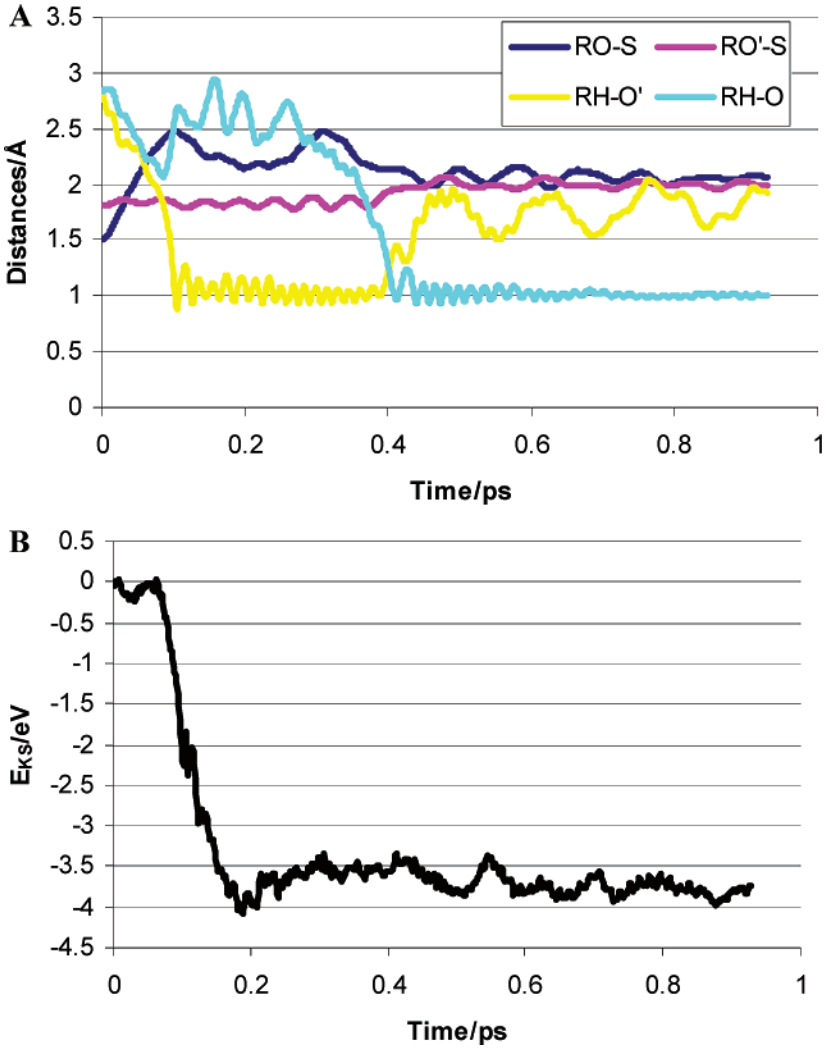

Figure 8. Time evolutions from CPMD trajectories of $OH_{ads} + O_{ads} + H_3O^+(H_2O)_2 + e^-$/Pt(111): (A) distances from the hydronium proton to the oxygen and to the hydroxyl oxygen, R_{H-O} and $R_{H-O'}$, and those between oxygen and hydroxyl oxygen and the surface, R_{O-S} and $R_{O'-S}$, respectively; (B) Kohn−Sham energy.

a negative background of equal magnitude.[28] The time evolutions of the Kohn−Sham energy are compared in Figure 6 for the cases with and without an electron included in the supercell. Without an electron in the simulation cell, for both initial distances of $R_{H-O} = 2.2$ and 2.5 Å, O_2 gets chemisorbed before the proton is transferred from the hydronium to O_2. This is in contrast to the case of the added electron, where the existence of the negative charge in the simulation cell (mainly distributed on the surface of the slab) facilitates the migration of the proton to the surface. Thus, with a slightly negative surface, the proton-transfer intermediate appears earlier than O_2 chemisorption for the cases with initial $R_{H-O} < 2.5$ Å.

The inset in Figure 6 illustrates the time evolutions of the net charge of the Pt slab for both cases. Considering that the electrode potential is one of the factors that determine the charge density of the surface, the two simulations emulate quite different electrode potentials. Nevertheless, for the given initial configurations, e.g., $R_{H-O} = 2.2$ and 2.5 Å, where the different surface charges lead to opposite electron- and proton-transfer sequences, the final product of the first electron reduction step is always a short-lived intermediate, O*OH, which readily decomposes into adsorbed OH and O.

3.1.4. Effect of Surface Relaxation. To address the reorganization effect of metal atoms on the ORR mechanism, CPMD simulations were also performed for $O_2 + H_3O^+(H_2O)_3 + e^- + Pt(111)$ with a relaxed top layer of the Pt slab. The trajectory qualitatively indicates a reaction mechanism rather similar to that found in the corresponding simulation with a fixed surface, i.e., chemisorption of O_2 followed by proton transfer and eventual decomposition of adsorbed OOH into coadsorbed O and OH.

Thus, on the basis of the CPMD simulations for typical initial configurations, the essential events for the ORR first electron reduction step in the presence of hydrated hydronium can be described as follows. A proton transfer is involved in the first reduction step, which qualitatively supports Damjanovic and Anderson's viewpoints.[6,14] Depending on the initial distance between proton and oxygen, on the surface charge, and on the degree of proton hydration, the proton transfer may precede or follow the electron transfer, bringing about an end-on and top-bridge chemisorbed H−O−O* species. Although the precursor has a defined lifetime of approximately 0.15 ps, it is unlikely that it is a stable intermediate as it was previously speculated. Instead, these results suggest a decomposition primarily driven by the chemisorption of hydroxyl, in line with Yeager's dissociative chemisorption proposal for the first step of ORR.[2] A unified mechanism for the first reduction step, which combines Damjanovic's proton participation in the first electron

reduction step and Yeager's dissociative chemisorption of O_2, is summarized as follows:

$$O_2 + H^+ \rightarrow OOH^+ \quad (1)$$

$$OOH^+ + * + e^- \rightarrow H-O-O^* \quad (2)$$

or

$$O_2 + * + e^- \rightarrow OO^-* \quad (3)$$

$$OO^-* + H^+ \rightarrow H-O-O^* \quad (4)$$

$$H-O-O^* + * \rightarrow HO^* + O^* \quad (5)$$

A Nafion membrane immersed in acid solution is widely used as the electrolyte in proton-exchange membrane fuel cells. The saturation water vapor uptake by Nafion 115 at ~350 K amounts to 18 wt %, and the mole ratio of water to sulfonate groups corresponds to 11.[37] It is generally accepted that there are a few distinct regions within the water-swollen membrane: a hydrophobic region made of the fluorocarbon backbone; a hydrophilic, ionic region mainly consisting of the sulfonate (SO_3^-), the hydrated protons, and the water of hydration; an intermediate between the two phases. The SO_3^- site may be surrounded by water molecules; despite the unknown exact degree of hydration, the proton can also be solvated by water molecules. For the models used here, $H_3O^+(H_2O)_{2,3}$, only the inner solvation shell was taken into account. Mulliken charge analysis for $H_3O^+(H_2O)_3(H_2O)_6$ shows that charges carried by protons decrease from H_3O^+ (~+0.46 e), to the waters in the inner shell (~+0.41 e), and to waters in the outer shell (~+0.31 e). Provided that the hopping channel as discovered in the section 3.1.2 is a major proton-transfer mechanism, the proton transfer could be weakened by the reduced electrostatic attraction between the hydrated proton and the adsorbed O_2. Reorganization energy of water molecules, including disruption and formation of H-bonds and H−O bonds, may increase the barrier of the proton transfer in eq 4, yielding that the decomposition of the adsorbed oxygen may precede the proton transfer. Indeed, CPMD simulations where the outer shell is taken into account by the model $H_3O^+(H_2O)_3(H_2O)_6$ predict this result. The details will be described elsewhere. Because of the limited number of water molecules, the question is whether the proton in the water swollen Nafion has so high degree of hydration, which depends on the competitive interactions of water with the (SO_3^-) site, and on the hydrogen bonding between the inner shell and outer shell waters. Thus, modeling hydrations of the SO_3^- site and of the proton for the optimal water uptake Nafion membrane electrolyte would be very helpful to investigate the ORR mechanism.

3.2. Second Electron-Transfer Step: O* + HO* + $H_3O^+(H_2O)_2$ + e^- and O*OH + $H_3O^+(H_2O)_2$ + e^-. Since the chemisorbed H−O−O* exists for approximately 0.15 ps, it is also likely that a second electron reduction takes place on this adsorbed species, which is speculated to be a primary path that could generate the intermediate HOOH. Thus, starting with the relatively stable intermediate (H−O−O*) and the products (O* and HO*) from the first reduction step, respectively, the second electron-transfer step of the ORR is explored by progressively loading $H_3O^+(H_2O)_2$ and an electron into the supercell.

Identical distances (2.83 Å) from the proton of $H_3O^+(H_2O)_2$ to O* and to the oxygen of HO* are set for the initial configuration (Figure 7a). Snapshots (Figure 7) and the time evolution of the distances (Figure 8) show that the proton migrates first to HO* probably due to the HO* oxygen bearing a higher negative charge, forming an intermediate H_2O adsorbed at an atop position (the distance between O and Pt is 2.10 Å) until 0.19 ps (Figure 7b). A barrier of approximately 0.2 eV was estimated from the graph of E_{KS} vs time, at 65 fs (Figure 8B), corresponding to the formation of H_2O^*. The proton transfer from H_3O^+ to adsorbed OH has been further confirmed by vibrational frequency analysis calculated with a Pt_3 cluster and the adsorbed species taken from the structure in Figure 7b (the imaginary frequency corresponding to the proton migration mode is 558 cm^{-1}). Within the following 0.2 ps, the dipole of H_2O^* gradually changes from perpendicular to nearly parallel to the Pt(111) surface (Figure 7c). One of the hydrogen atoms of H_2O^* also gets closer toward O*, and a strong hydrogen bond gradually occurs between H_2O^* and O*. It is the hydrogen bond that catalyzes the proton transfer, and two HO*'s eventually appear at an atop position (Figure 7d). The result is in good agreement with that based on ab initio cluster theoretical analysis, by which two atop coadsorbed HO are more stable than coadsorbed water and oxygen.[36] A hydrogen bond is observed between two atop adsorbed hydroxyls (Figure 7d), and this may be responsible for the stability of two atop-adsorbed hydroxyls at adjacent sites during the remaining of the CPMD simulation. Although the properties of adsorbed hydroxyls may differ depending on the way they were generated on the surface and on their degree of coverage, Hu et al.[30] also found that hydrogen bonding between adjacent hydroxyl groups at high coverage ($^1/_2$ to 1 ML) leads to a strong preference of OH adsorption at top sites.

From the analysis of CPMD simulations starting with H−O−O* (Figure 9a), it is observed that the proton of $H_3O^+(H_2O)_2$ migrates to the oxygen close to the Pt(111), as indicated by the evolution of the distance (R_{H-O1}) between the proton and the oxygen shown in Figure 10A. The result is a one end adsorbed hydrogen peroxide, HOO*H, at approximately 0.16 ps (Figure

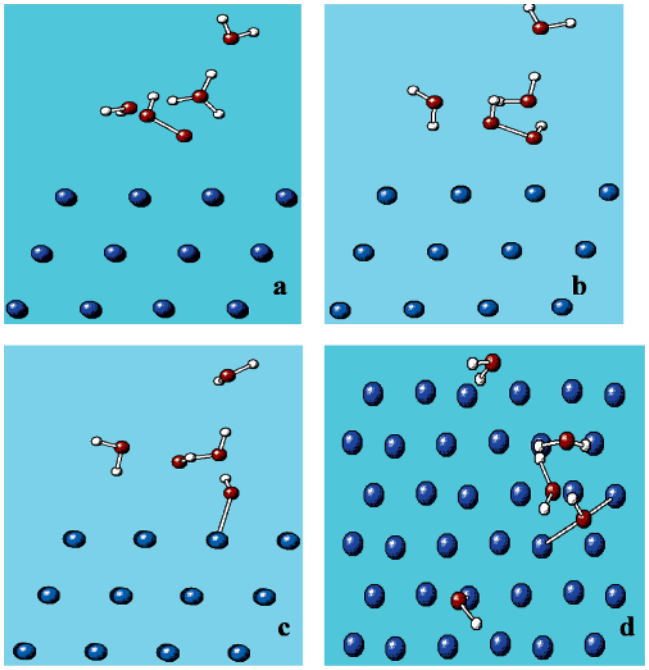

Figure 9. CPMD snapshots of (OOH + $H_3O^+(H_2O)_2$ + e^-)/Pt(111) at 350 K: (a) side view of the initial configuration where the hydronium proton is separated from the oxygen end by 3.0 Å; (b) an end-on HOOH formed at 0.15 ps, R_{O-O} ~ 1.50 Å; (c) dissociation of the end-on-adsorbed HOOH observed at 0.22 ps, R_{O-O} ~ 2.30 Å; (d) top view of the configuration excluding the water molecules at 0.69 ps, where two hydroxyls are respectively adsorbed on a top and a bridge site.

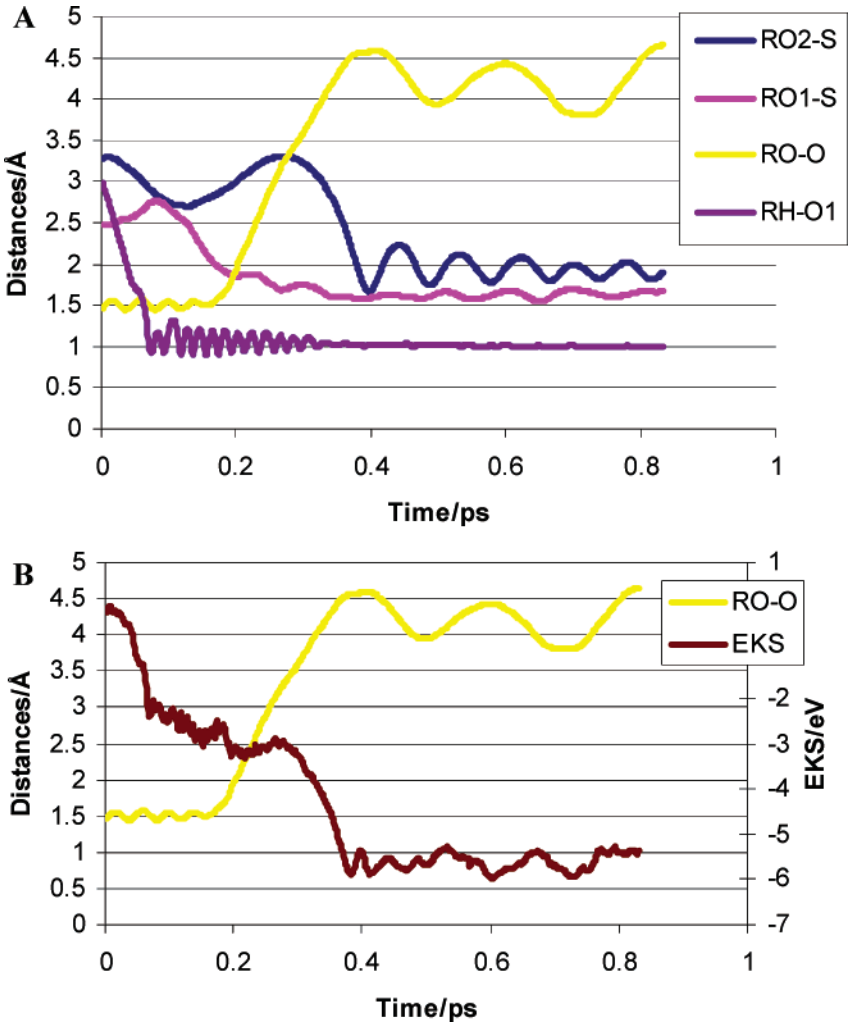

Figure 10. CPMD time evolutions of (HOO + $H_3O^+(H_2O)_2$ + e^-)/Pt(111): (A) distances between the hydronium proton and the oxygen end of OOH (R_{H-O1}), those of the OOH oxygen atoms above the Pt(111) surface (R_{O1-S} and R_{O2-S}), and the O−O bond length (R_{O-O}); (B) Kohn−Sham energy (E_{KS}) and R_{O-O}.

9b), where the O*O bond length is 1.5 Å, and the distance between O* and the adsorbent Pt atoms is 2.10 Å. Cluster DFT optimizations also confirm the presence of adsorbed HOO*H, as discussed elsewhere.[36] However, the lifetime of HOO*H is quite short. As shown by Figure 9, HOO*H dissociates homolytically into a weakly adsorbed hydroxyl (O2H; see Figure 9c) and a top chemisorbed hydroxyl (O1H). According to Figure 10B, a barrier of approximately 0.4 eV accompanies such decomposition at 0.18 ps. Thereafter, the R_{O-O} distance (Figure 10B) continuously increases until 0.4 ps and then vibrates around 4.2 Å. O2H begins to get close to the Pt(111) surface at 0.28 ps and then adsorbs at a top site accompanied by a rapid decrease of E_{KS} (Figure 10B). O1H diffuses over the Pt(111) surface with an estimated barrier of 0.2 eV and eventually is adsorbed at a bridge site after the complete decomposition of HOOH (Figure 9d), where the distances between O1H and its two neighbor adsorbing Pt atoms are 2.15 ± 0.1 Å, whereas the oxygen of O1H is around 1.6 Å over the Pt(111) surface (R_{O1-S}). OH adsorption at the bridge site has been also often reported, especially at low surface coverage or in absence of neighbor coadsorption.[30,38]

It is known that some amount (0−20%, depending on the applied potential) of hydrogen peroxide can be formed as either a product or an intermediate on Pt(111) surfaces.[17,18] The present CPMD simulations suggest that a one-end adsorbed hydrogen peroxide, HOO*H, is most likely to be generated. However, it has relatively short lifetime and readily dissociates homolytically into HO and HO* before the other oxygen atom gets chemically adsorbed to form a dual adsorbed HO*O*H. In other words, similarly to O*OH, dissociative adsorption also takes place on the end-on HOO*H species, and it is the chemisorption that drives the dissociation of HOO*H.

On the basis of the above discussion, the suggested mechanisms for the competitive elementary reactions of H−O−O* are

$$\mathrm{HOO^* + H^+ + e^- \rightarrow HOO^*H} \quad (6)$$

$$\mathrm{HOO^*H + * \rightarrow HO^* + HO^*} \quad (7)$$

and

$$\mathrm{H{-}O{-}O^* + * \rightarrow HO^* + O^*} \quad (5)$$

$$\mathrm{O^* + HO^* + H^+ + e^- \rightarrow H_2O^* + O^*} \quad (8)$$

$$\mathrm{H_2O^* + O^* \rightarrow 2HO^*} \quad (9)$$

Among the three possible reduction products of HOO*, HOO*H from the direct reduction, i.e., reaction 6, is the least stable thermodynamically, followed by the coadsorbed O* and H_2O^* from indirect reduction (i.e., first dissociation and then

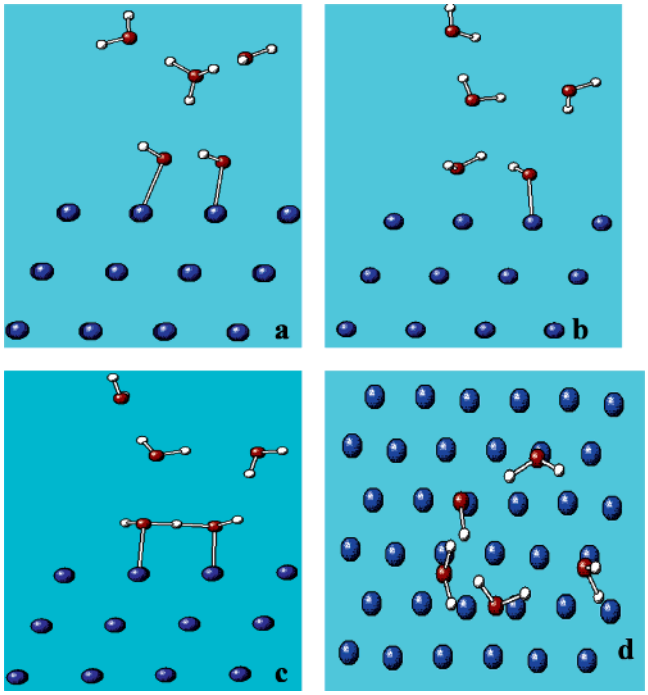

Figure 11. CPMD snapshots of (2HO* + $H_3O^+(H_2O)_2$ + e^-)/Pt(111) at 350 K: (a) side view of the initial configuration where the hydronium proton is separated from the hydroxyl oxygen by 3.0 Å; (b) water dipole tending to be parallel to the Pt(111) surface at 0.42 ps; (c) proton shared by two hydroxyls at 0.53 ps, where the distances between the shared proton and the two hydroxyl oxygen atoms are 1.15 and 1.33 Å, respectively; (d) shared proton transferred at 0.71 ps.

reduction, reactions 5 and 8), whereas the formation of two coadsorbed HO* is the most stable.

3.3. Third Electron-Transfer Step: 2HO* + $H_3O^+(H_2O)_2$ + e^-. With addition of $H_3O^+(H_2O)_2$ and an e^- into the cell containing the HO* + HO* from the second reduction step on the Pt slab (Figure 11a), the third electron-transfer step is investigated. In the initial configuration, the hydronium proton is equidistant at 2.6 Å from the two atop-adsorbed hydroxyl oxygen atoms. Likewise, the CPMD trajectory shows that the proton rapidly migrates to HO*, forming an intermediate H_2O* at 0.18 ps, where the proton from $H_3O^+(H_2O)_2$ does not completely leave the hydronium ion (the distance between proton and water oxygen is 1.47 Å). The intermediate then transforms to H_2O* by dehydration of the proton, and the adsorbed water tends to be flat on the Pt(111) surface, which favors hydrogen bonding between H_2O* and OH* (Figure 11b).

As time evolves, a hydrogen-bonded radical [(HO*−H−O*H)•] is generated (Figure 11c), which is almost centrosymmetric with respect to the shared proton (∼1.2−1.3 Å from each oxygen atom); the H-bond is found in a nonlinear O···H···O arrangement (angle OHO ∼ 150°; R_{O-O} ∼ 2.4−2.5 Å). The geometry and electronic structure of the charged water complex $H_3O_2^-$ have been extensively investigated,[39,40] whereas little has been reported on the structure of the radical H_3O_2•. The minimum energy configuration of $H_3O_2^-$ presents a shared proton with one covalent OH bond forming an asymmetric $[HO-H\cdots O]^-$ complex (∼1.089 and 1.426 Å from the shared proton to each oxygen atom in a nearly linear O−H···O arrangement calculated with MP2/aug-cc-pVDZ),[40] which has slightly lower energy (by 0.3 kcal/mol) than the symmetric structure $[HO\cdots H\cdots OH]^-$ (the first-order saddle point) at zero temperature. The asymmetric analogue of free H_3O_2• cannot be predicted by MP2, whereas the structure [HO···H···OH]• with a centrosymmetric shared proton (∼1.15 Å from each oxygen

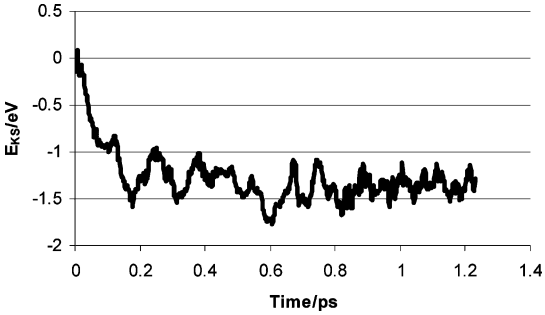

Figure 12. E_{KS} evolution from CPMD simulations of the system (2HO* + $H_3O^+(H_2O)_2$ + e^-)/Pt(111).

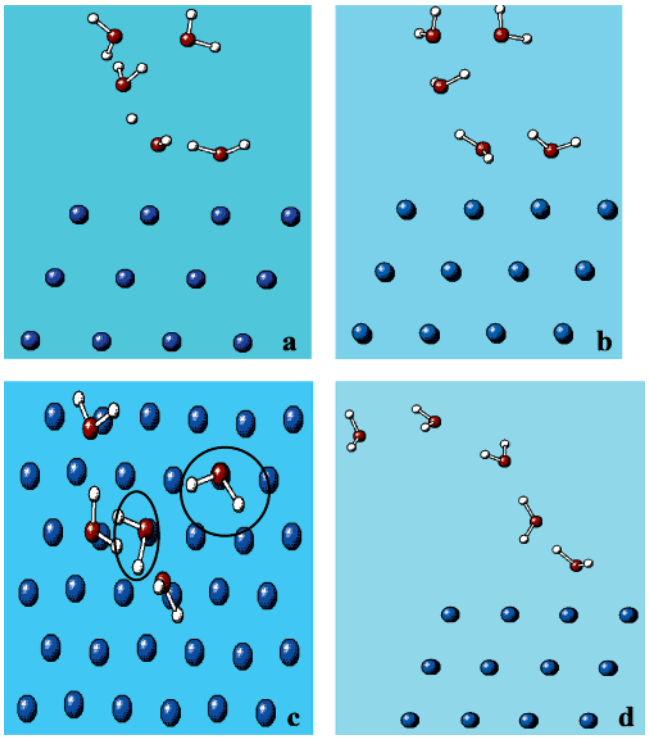

Figure 13. CPMD snapshots of (HO* + H_2O* + $H_3O^+(H_2O)_2$ + e^-)/Pt(111) at 350 K: (a) side view of the configuration at 0.072 ps, where the hydronium proton is already between the water molecule and the hydroxyl; (b) water adsorbed in an almost flat configuration on top of the Pt(111) surface at 0.16 ps; (c) top view at 0.29 ps, where two adsorbed waters (circled) have a hydrogen bond with a O···H distance of 1.87 Å; (d) one water molecule desorbed at 0.52 ps. A configuration at 1.0 ps shows a hydrogen-bond network among water molecules.

with an angle OHO of 140.4°) is a local minimum that is less stable than a weakly hydrogen bonded complex $[H_2O\cdots HO]$• by 13.8 kcal/mol at MP2/aug-cc-pVDZ. This result is consistent with the information obtained from the E_{KS} (Figure 12) for the absorbed H_3O_2•, including the electronic energy difference.

For the third electron step, the above CPMD simulation shows that the hydroxyl is reduced to an atop-adsorbed water,

$$HO^* + HO^* + H^+ + e^- \rightarrow H_2O^* + HO^* \qquad (10)$$

During the remaining simulation, water desorption was not found probably due to adsorption on the surface as well as to the hydrogen bonding with the adjacent HO*.

3.4. Fourth Electron-Transfer Step: H_2O*+O*H+$H_3O^+(H_2O)_2$ + e^-. If one starts with atop-coadsorbed H_2O* and O*H, the fourth electron transfer step is finally explored with further uploading $H_3O^+(H_2O)_2$ and an e^- to the supercell. The snapshots of key configurations and the time evolution of E_{KS} together

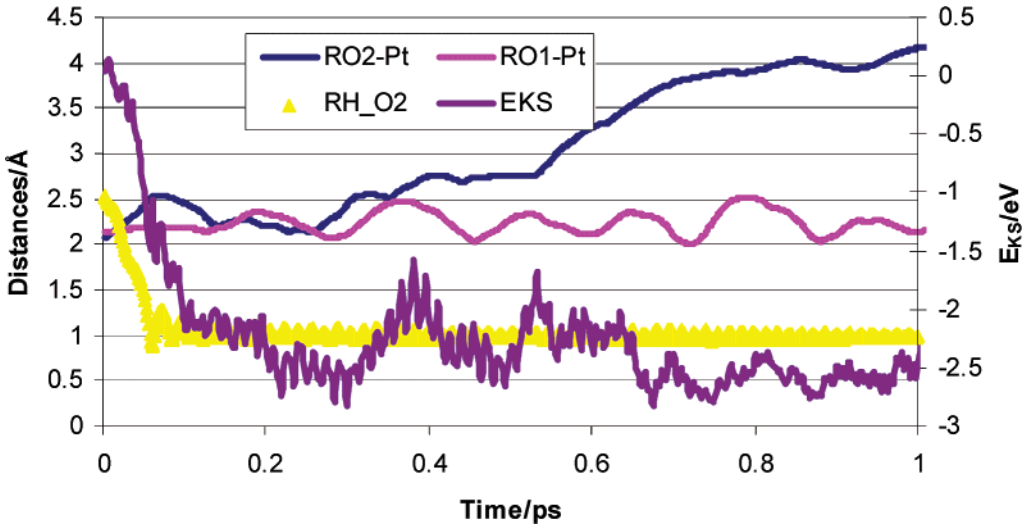

Figure 14. Time evolution from CPMD simulations of (OH_{ads} + H_2O_{ads} + $H_3O^+(H_2O)_2$ + e^-)/Pt(111): distances between the hydronium proton and the oxygen end of OH (R_{H-O2}), those between the oxygen atoms of OH_{ads} and H_2O_{ads} and the adsorbing Pt atoms (R_{O1-Pt} and R_{O2-Pt}), and Kohn−Sham energy of the system (E_{KS}).

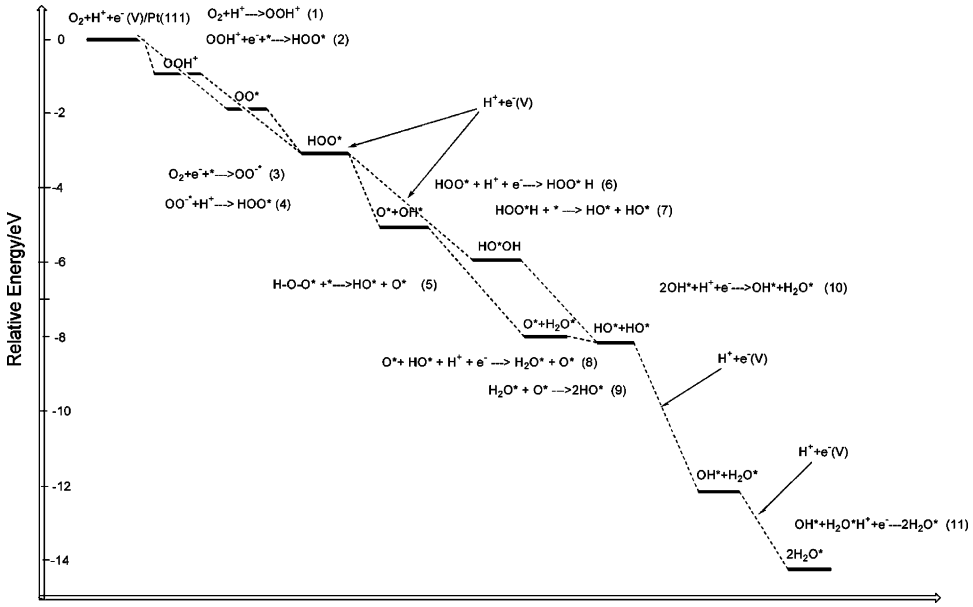

Figure 15. Reaction pathway profile of the oxygen reduction reaction on Pt(111). The reference states are O_2 + H^+ + e^- (V)/Pt(111) for the first electron reduction step and either the products or the intermediates from the previous reduction steps together with H^+ + e^- (V)/Pt(111) for the other reduction steps. The pathway is dependent on the electrode potential e^- (V).

with those of various characteristic distances are shown in Figures 13 and 14, respectively. The proton of $H_3O^+(H_2O)_2$ is initially set to be at a distance of ∼2.6 Å from the hydroxyl oxygen, and it rapidly migrates to the hydroxyl oxygen forming partially adsorbed H_2O at 0.1 ps. The proton transfer is accompanied by the increase of R_{HO2-Pt} (the distance between the hydroxyl oxygen and the adsorbing Pt atom) by ∼0.5 Å and by a remarkable E_{KS} decrease of ∼2.2 eV mainly due to water formation. Over the following 0.15 ps period, the newly formed water (W2) gradually gets atop adsorbed on the Pt(111) surface in a nearly flat configuration as shown in Figure 13b (R_{HO2-Pt} ∼ 2.2 Å) and also forms a hydrogen bond with the other existing water molecule (denoted as W1), which are mainly responsible for the E_{KS} decrease of 0.5 eV (Figure 14). The binding energy of a single water molecule on Pt(111) was reported to be ∼0.3 eV calculated with periodic DFT (O−Pt ∼ 2.4 Å),[41] and ∼0.6 eV with a Pt_{3-6} cluster using DFT (O−Pt ∼ 2.3 Å).[36] W2 begins to desorb from the Pt(111) surface at 0.29 ps, with an estimated energy barrier of ∼0.6 eV (Figure 14), and the R_{HO2-Pt} distance reaches ∼2.7 Å at 0.53 ps with a tilted configuration (Figure 13d), whereas W1 is always atop adsorbed in a flat configuration with R_{HO1-Pt} fluctuating around 2.2 Å (Figure 14).

4. Summary

CPMD simulations have been performed to investigate the ORR mechanism on a Pt(111) surface in the presence of a hydrated proton. Figure 15 shows the elementary reaction pathways together with the Kohn−Sham electronic energy. The developed elementary reactions can be used as a working mechanism to perform kinetic Monte Carlo simulations. New insights about the ORR are observed which are summarized as follows:

(a) A proton transfer is involved in the first reduction step as previously suggested.[6,14] Depending on the initial distance between the proton and the molecular oxygen, on the surface charge, and on the degree of proton hydration, the proton transfer

can either precede or follow O_2 chemisorption, in all cases forming an end-on complex H−O−O*. Although H−O−O* has a finite lifetime of approximately 0.15 ps, it is unlikely that it is a stable intermediate as previously speculated. Instead, its decomposition will occur primarily driven by chemisorption of hydroxyl, which is in line with Yeager's dissociative chemisorption proposal for the ORR first step.[2]

(b) In the second reduction step, formation of the one-end adsorbed hydrogen peroxide, HOO*H, is indeed observed via the direct reduction of H−O−O*, which suggests that the ORR may also proceed via HOO*H, i.e., series pathway. However, it readily dissociates homolytically into two coadsorbed hydroxyls (HO* + HO*) rather than forming a dual adsorbed HO*O*H. The other path for the second reduction step is that coadsorbed O* and HO* from the dissociation of H−O−O* is first reduced to an atop adsorbed water and O* and proton transfer then happens with the help of the hydrogen bonding between water and the adjacent adsorbed oxygen, bringing about two atop-adsorbed hydroxyls in neighbor sites. Both from thermodynamics and kinetics grounds, the end-on chemisorption precursor H−O−O* from the first reduction step has a strong tendency to decompose. In addition, the intermediate from series pathway HO*OH is much less stable than O* + H_2O*, yielded by the direct pathway. Therefore, the second path for the second electron transfer of ORR should be dominant. It is theoretically validated that the O_2 reduction on a Pt(111) surface may proceed by a parallel pathway with the direct as the dominant step.

(c) For the third reduction step, the CPMD simulation starting with two atop-adsorbed hydroxyls (HO* + HO*) in adjacent sites shows that one of the hydroxyls is first reduced to atop adsorbed water. The hydrogen bonding between the newly formed water and the hydroxyl promotes the proton transfer, forming a defect configuration, $[HO\cdots H\cdots OH]^{\bullet}$, wherein the shared proton is strongly hydrogen bonded with two atop-adsorbed hydroxyls. The system is finally stable with atop-adsorbed water and hydroxyl species. During the remaining simulation, water desorption was not found probably due to adsorption on the surface as well as the hydrogen bonding with the adjacent HO*.

(d) The fourth ORR reduction step generates the end product, two atop-adsorbed water molecules. During the present simulations, one water desorption event was observed, which was accompanied by a considerable energy increase of approximately 0.6 eV.

Acknowledgment. Financial support from the Department of Energy/Basic Energy Sciences (Grant DE-FG02-04ER15619) and from DURIP/ARO (Grant No. W911N F-04-1-0098) is gratefully acknowledged. The use of computational facilities at the NSF HPC and TeraGrid Sites, National Center for Supercomputing Applications (Grant CHE040052), and at the National Energy Research Scientific Computing Center, NERSC, is appreciated.

References and Notes

(1) Damjanovic, A.; Brusic, V. *Electrochim. Acta* **1967**, *12*, 615.
(2) Yeager, E. B. *Electrochim. Acta* **1984**, *29*, 1527.
(3) Adzic, R. In *Electrocatalysis*; Lipkowski, J., Ross, P. N., Eds.; Wiley-VCH: New York, 1998; p 197.
(4) Markovic, N. M.; P. N. Ross, J. *Surf. Sci. Rep.* **2002**, *45*, 117.
(5) Anderson, A. B.; Albu, T. V. *J. Electrochem. Soc.* **2000**, *2000*, 4229.
(6) Sidik, R. A.; Anderson, A. B. *J. Electroanal. Chem.* **2002**, *528*, 69.
(7) Xu, Y.; Ruban, A. V.; Mavrikakis, M. *J. Am. Chem. Soc.* **2004**, *126*, 4717.
(8) Murthi, V. S.; Urian, R. C.; Mukerjee, S. *J. Phys. Chem. B* **2004**, ASAP.
(9) Steele, B. C. H.; Heinzel, A. Materials for Fuel-Cell Technologies. *Nature* **2001**, *414*, 345.
(10) Markovic, N. M.; Schmidt, T. J.; Stamenkovic, V.; Ross, P. N. *Fuel Cells* **2001**, *1*, 105.
(11) Yeager, E.; Razaq, M.; Gervasio, D.; Razaq, A.; Tryk, D. *Proc. Workshop Struct. Eff. Electrocatal. Oxygen Electrochem.* **1992**.
(12) Clouser, S. J.; Huang, J. C.; Yeager, E. B. *J. Appl. Electrochem.* **1993**, *23*, 597.
(13) Yeager, E. R., M.; Gervasio, D.; Razaq, A.; Tryk, D. Dioxygen reduction in various acid electrolytes. *J. Serb. Chem. Soc.* **1992**, *57*, 819.
(14) Damjanovic, A.; Sepa, D. B.; Vojnovic, M. V. *Electrochim. Acta* **1979**, *24*, 887.
(15) Sepa, D. B.; Vojnovic, M. V.; Vracar, L. M.; Damjanovic, A. *Electrochim. Acta* **1987**, *32*, 129.
(16) Wang, Y. B., Balbuena, P. B. *J. Phys. Chem. B* **2004**, *108*, 4376.
(17) Stamenkovic, V.; Schmidt, T. J.; Ross, P. N.; Markovic, N. M. *J. Phys. Chem. B* **2002**, *106*, 11970.
(18) Nakanishi, S.; Mukouyama, Y.; Karasumi, K.; Imanishi, A.; Furuya, N.; Nakato, Y. *J. Phys. Chem. B* **2000**, *104*, 4181.
(19) Car, R.; Parrinello, M. *Phys. Rev. Lett.* **1985**, *55*, 2471.
(20) *CPMD*, 3.7.2 ed.; IBM Corp., 1990−2004, MPI fuer Festkoerperforschung, Stuttgart, Germany, 1997−2001, 2003.
(21) Becke, A. D. *Phys. Rev. A* **1988**, *38*, 3098.
(22) Lee, C.; Yang, W.; Parr, R. G. *Phys. Rev. B* **1988**, *37*, 785.
(23) Troullier, N.; Martins, J. L. *Phys. Rev. B* **1991**, *43*, 1993.
(24) Hirshfeld, F. L. *Theor. Chim. Acta* **1977**, *44*, 129.
(25) Michaelides, A.; Hu, P. *J. Am. Chem. Soc.* **2001**, *123*, 4235.
(26) *Handbook of Chemistry and Physics*; 77th ed.; Lide, D. R., Ed.; CRC Press: Boca Raton, FL, 1997.
(27) *Handbook of Chemistry and Physics*, 67th ed.; Weast, C. R., Ed.; CRC Press: Boca Raton, FL, 1986.
(28) Marx, D.; Sprik, M.; Parrinello, M. *Chem. Phys. Lett.* **1997**, *273*, 360.
(29) Adzic, R. R.; Wang, J. X. *J. Phys. Chem. B* **1998**, *102*, 8988.
(30) Michaelides, A.; Hu, P. *J. Chem. Phys.* **2001**, *114*, 513.
(31) Bedurftig, K.; Volkening, S.; Wang, Y.; Wintterlin, J.; Jacobi, K.; Ertl, G. *J. Chem. Phys.* **1999**, *111*, 11147.
(32) Balbuena, P. B.; Altomare, D.; Vadlamani, N.; Bingi, S.; Agapito, L. A.; Seminario, J. M. *J. Phys. Chem. A* **2004**, *108*, 6378.
(33) Koper, M. T. M.; van Santen, R. A. *J. Electroanal. Chem.* **1999**, *472*, 126.
(34) Lin, X.; Ramer, N. J.; Rappe, A. M.; Hass, K. C.; Schneider, W. F.; Trout, B. L. *J. Phys. Chem. B* **2001**, *105*, 7739.
(35) Li, T.; Balbuena, P. B. *J. Phys. Chem. B* **2001**, *105*, 9943.
(36) Wang, Y. X.; Balbuena, P. B. *J. Chem. Theory Comput.*, in press.
(37) Yang, C.; Srinivasan, S.; Bocarsly, A. B.; Tulyani, S.; Benziger, J. B. *J. Membr. Sci.* **2004**, *237*, 145.
(38) Koper, M. T. M.; Shubina, T. E.; van Santen, R. A. *J. Phys. Chem. B* **2002**, *106*, 686.
(39) Tuckerman, M. E.; Marx, D.; Klein, M. L.; Parrinello, M. *Science* **1997**, *275*, 817.
(40) Xantheas, S. S. *J. Am. Chem. Soc.* **1995**, *117*, 10373.
(41) Meng, S.; Xu, L. F.; Wang, E. G.; Gao, S. *Phys. Rev. Lett.* **2002**, *89*, 176104.